Investigation of non-halogenated solvent mixtures for high throughput fabrication of polymer-fullerene solar cells

Benjamin Schmidt-Hansberg[a*], *Monamie Sanyal*[b], *Nadia Grossiord*[c], *Yulia Galagan*[c], *Michael Baunach*[a], *Michael F.G. Klein*[d], *Alexander Colsmann*[d], *Philip Scharfer*[a], *Uli Lemmer*[d], *Helmut Dosch*[e], *Jasper Michels*[c], *Esther Barrena*[b,f**], *Wilhelm Schabel*[a]

[a] Institute of Thermal Process Engineering, Thin Film Technology, Karlsruhe Institute of Technology (KIT), Kaiserstraße 12, D-76131 Karlsruhe, Germany

[b] Max Planck Institut für Metallforschung, Heisenbergstrasse 3, 70569 Stuttgart, Germany

[c] Holst Centre/TNO, PO Box 8550, 5605 KN Eindhoven, The Netherlands

[d] Light Technology Institute, Karlsruhe Institute of Technology (KIT), Kaiserstraße 12, D-76131 Karlsruhe, Germany

[e] Deutsches Elektronen-Synchrotron (DESY), Notkestr. 85, D-22607 Hamburg, Germany

[f] Institut de Ciencia de Materials de Barcelona (ICMAB-CSIC), 08193 Bellaterra, Spain

Corresponding author * schmidt-hansberg@kit.edu, ** ebarrena@icmab.es

ABSTRACT

The rapidly increasing power conversion efficiencies of organic solar cells are an important prerequisite towards low cost photovoltaic fabricated in high throughput. In this work we suggest indane as non-halogenated replacement for the commonly used halogenated solvent o-dichlorobenzene. Indane was blended with the higher volatile solvents chloroform or toluene or o-xylene in order to improve wettability and to reduce drying time. The combination of high volatile solvents with the less volatile host solvent indane allows for an increased fabrication speed due to a reduction of the overall drying time and provides films with good light absorption behavior and high polymer crystallinity. For the solvent mixture toluene-indane, solar cell performance is comparable to the o-dichlorobenzene reference device indicating this mixture as a suitable replacement for increased productivity without drawbacks in nanomorphology as investigated by atomic force microscopy (AFM) and grazing incidence X-ray diffraction (GIXD). This study provides a fundamental understanding on solvent mixture drying kinetics and can aid the ink formulation.

KEYWORDS: organic photovoltaic, drying process, P3HT:PCBM, morphology, grazing incidence X-ray diffraction (GIXD), knife coating

1. Introduction

The performance of organic solar cells has made rapid progress in the past years by reaching 9.2% power conversion efficiency recently. [1] The intrinsic advantages of solution processable and mechanically flexible materials allows the realization of flexible [2-5], stretchable [6] solar cells or even textile fibers [7]. For large area fabrication of such devices different techniques such as knife over roll coating [8], slot die coating [8-11], screen printing [5, 8-10, 12, 13] and gravure coating [9, 14] could be utilized.

Large area solution processing also involves the evaporation of large amounts of solvents. These are commonly halogenated which can cause difficulties for industrial applications due to their toxicity. In the scope of high throughput manufacturing it is therefore desirable to use non-halogenated solvents. The very limited solubility of organic semiconductors complicates the replacement of the usual solvents like chlorobenzene and o-dichlorobenzene (DCB). Besides a sufficiently high solubility, the solvent must also allow appropriate structure formation of the polymer-fullerene blend during film drying. For good energy conversion efficiency the dry polymer-fullerene blend must ideally comprise a multiple scale phase separated, interpenetrating polymer-fullerene network with crystalline polymer domains and with percolation pathways within each material to the electrodes. [15-18] Slow drying was reported as one of the methods to enhance the order of P3HT in P3HT:PCBM blends resulting in an improved solar cell efficiency [19-21]. However, slow drying results in low throughput due to slow coating speeds or extremely long driers at high coating speeds. Additionally, slow drying provides time for dewetting processes which can be kinetically suppressed at fast drying conditions and the wet surface collects ambient dust

particles. Therefore, the reduction of drying time is beneficial for an efficient high throughput solar cell fabrication process.

In this work, we report the successful replacement of DCB with a non halogenated solvent indane that delivers power conversion efficiencies of poly-(3-hexylthiophene-2,5-diyl) (P3HT) and C_{61}-butyric acid methyl ester (PCBM) doctor-bladed solar cells close to the DCB reference devices. Moreover, the incorporation of a higher volatile component results in an initially accelerated drying followed by a final slow drying period (the latter needed for molecular ordering. [19-22]) Case studies of drying kinetics for a set of different volatile solvents provide a fundamental understanding of solvent mixture drying kinetics. The dried films have been characterized by grazing incidence X-ray diffraction (GIXD) and atomic force microscopy (AFM).

The combination of high volatile solvents with the less volatile host solvent indane allows for an increased fabrication speed due to a 40% reduction of the overall drying time and provides films with good light absorption behavior, high P3HT crystallinity and efficient device performance. This study can aid the ink formulation for environmentally friendlier solvent mixtures.

2 Methods

2.1 Numerical Approach for Drying Kinetics

For aiding ink formulation, drying kinetics simulations of the mentioned solvent mixtures have been accomplished. These calculations are done for horizontal plate geometry in forced convection by a two dimensional mass transfer model including a moving drying front as described in previous work. [23, 24] The calculations are carried out with an

initially uncoated offset of x_0=10mm which is followed by 60 mm wet film of x_{solid}=2wt% solid fraction of P3HT:PCBM ($x_{solvent}$=98 wt.%) and 200 nm dry film thickness. Drying kinetics are shown for the centered position of the wet film, i.e. at x=30mm. Drying conditions are 20°C and v=0.3 m/s drying gas velocity. The simulations cover the constant rate drying period regime, where diffusional mass transfer limitations of solvent in the film can be neglected. The drying kinetics simulation of the last few nanometers, which is called falling rate drying period, would additionally require the determination of solvents diffusion coefficients in the P3HT:PCBM matrix as a function of the solvent concentration. Changes in the drying gas flow rate will only affect the overall drying time but the characteristic of the evolution of $x_{solvent}$ remains alike. P3HT and PCBM solubility have been determined as described in reference [21].

2.2 Experimental

P3HT:PCBM solar cells were fabricated by dissolving 1.5 wt.% of P3HT (M_w =58900 g/mol, PDI = 1.9, Rieke Metals, 4002E) and 1.2 wt.% of PCBM (purity >99%, Solenne BV) at 70˚C for 14 hours in several solvent systems, namely o-dichlorobenzene (DCB), indane, as well as 1:1 by wt. mixtures of toluene-indane, o-xylene-indane and chloroform-indane. Chloroform and toluene were purchased from Merck, whereas o-xylene (98%), DCB (99%), and indane (95%) were provided by Sigma-Aldrich.

After cleaning the 3×3 cm² pre-patterned-ITO glass substrates (Philips polyLED), poly(3,4-ethylenedioxythiophene) doped with poly(styrenesulfonate) (PEDOT:PSS, Clevios P VP Al 4083 provided by Heraeus Clevios GmbH) was spin-coated, and annealed at 130 ˚C for 6 minutes. The thickness of the resulting PEDOT:PSS layer was 50 nm, as measured with a

Dektak profilometer. The photoactive layer (PAL) was subsequently deposited by the doctor blade technique (Coatmaster 509 MC-1). Solvent evaporation was allowed to proceed slowly by covering the just deposited PAL with a Petri dish. Finally, the top electrode, made of 1 nm LiF and 100 nm Al, was thermally evaporated in a vacuum chamber through a shadow mask, with an active area of 0.167 cm^2.

X–ray reflectivity and GIXD measurements were performed on P3HT:PCBM solar cell devices in the synchrotron facility ANKA (Karlsruhe, Germany), using a point detector with 8 keV photon energy. 2D GIXD measurements were conducted with an area detector (MarCCD) at 12.3keV at beamline ID10B in the European Synchrotron Radiation Facility (ESRF, Grenoble, France). AFM measurements were done in tapping mode with a Veeco Dimension Icon.

The absorption spectra were measured in transmission with a spectrophotometer (Perkin Elmer, Lambda 1050) using a blank PEDOT:PSS/ITO/glass substrate as reference. The absorption spectra are normalized to the PCBM absorption peak at 333 nm.

The current-voltage characteristics were recorded with a Keithley 2400 sourcemeter, using a 50-W halogen lamp with IR filter, resulting in mismatch factor of 0.75. Prior to measurements, the light source was calibrated to 1 sun intensity with a standard Si photodiode detector. Each $3\times3\ cm^2$ substrate contained 4 solar cells. Current-voltage characteristics were measured before and after the cells underwent a thermal treatment at 130˚C for 5 minutes.

3. Results and Discussion

3.1 Film Drying Kinetics

In preceding work we have demonstrated that the P3HT:PCBM blend crystallization in DCB proceeds with primary P3HT crystallization at solvent fractions of $x_{solvent}$=85-95 wt.% (after crossing the P3HT solubility limit) followed by PCBM clustering in the final drying period at low solvent fractions $x_{solvent}$ < 55wt%.[21] The observation of a delay in P3HT crystallization leads to the assumption that this period -before crossing the solubility limit- does not contribute significantly to structure formation. Hence, it seems likely that skipping this initial phase by faster drying will result in comparably performing solar cells. This consideration leads us to investigate the combination of high volatile solvents chloroform (bp = 61°C), toluene (bp = 111°C) and o-xylene (bp = 144°C) with the less volatile host solvent indane (bp = 178°C). Vapor pressure of the environmentally friendlier indane and its solubility of P3HT and PCBM are comparable to the well known ideal solvent DCB (bp = 179°C). For indane P3HT and PCBM solubility at 20°C was determined to 2.9 wt% and 5.5 wt% respectively (the solubility of P3HT and PCBM at 20°C in DCB is 3.8 wt% and 2.6 wt% respectively). Higher PCBM solubility represents higher solid-solvent interaction forces for PCBM which might reduce polymer-fullerene interaction in indane solution in comparison to DCB. Implications on film morphology will be discussed in the structural section.

Figures 1a-c depict the calculated evolution of solvent mass fraction $x_{solvent}=(m_{solv.1} + ms_{olv.2})/(m_{solv.1} + ms_{olv.2} + m_{solid})$ of drying P3HT:PCBM films for different solvent blending ratios of chloroform-indane, toluene-indane and o-xylene-indane. Figure 1d shows the drying path through the quasi ternary phase diagram for the investigated P3HT:PCBM.

For easier readability, the mass fractions of the solvent mixtures are reflected as a single solvent. The drying kinetics for pure indane (0:1 solvent ratio) is governed by a slow decrease of solvent mass fraction x_{solv} in the beginning. This leads to a long residence time at solvent fractions >85 wt%, similar to the case of DCB. [23, 24] As the solid fraction becomes significant, the solvent fraction x_{solv} reduces rapidly and a wide range in the phase diagram is crossed quickly leading to the blend crystallization. In the top row of Figure 1a-c it gets quantitatively clear, that the overall drying time can be influenced by the type of solvent combination in the mixture and the solvent blending ratio. In addition the mixture of indane with high volatile solvents causes a faster drying at the initial stage as it can be observed in the zoomed plots shown in the bottom row of Figure 1a-c.

Due to lower differences in the vapor pressure of the mixture o-xylene-indane in Figure 1c, no abrupt change in the evaporation kinetics can be detected. For the 1:1 solvent blending ratio the transition from fast to slower indane dominated drying kinetics has largely completed at 95-96 wt% overall solvent fraction. This secures that the initially fast drying period has ended roughly at the P3HT:PCBM solubility limit. Hence, for this solvent blending ratio a reduction of retention time is attained in that area of the phase diagram, where no crystallization processes are proceeding. Beside the slightly increasing drying time, from chloroform to toluene and o-xylene due to the decreasing vapor pressure, one can see a strong difference in the sharpness of the transition from initially fast to slower drying period. Figure 1e shows the evolution of film thickness during drying for the 1:1 solvent mixtures.

Aiming for high fabrication throughput, fast drying is desired. Since the solvent mixture chloroform-indane exhibits the fastest drying kinetics this would be the best candidate for

fast production, but chloroform is not the desired non-halogenated replacement for DCB. In the following we will discuss how far the choice of solvent mixtures in combination with their evaporation kinetics influences the film structure and the corresponding optoelectronic properties of solar cells.

3.2 Film Structure for Different Solvent Mixtures

For the structural characterization, we have performed X-ray diffraction and AFM measurements of P3HT:PCBM solar cells. Figure 2a depicts the 2D GIXD diffraction pattern of a P3HT:PCBM film on a glass/ITO/PEDOT:PSS substrate cast by doctor blade from a toluene-indane mixture. While PCBM exhibits a powder like diffraction ring of randomly oriented aggregates, P3HT shows a predominant edge-on configuration, i.e with (100) oriented perpendicular to the substrate and (020) oriented in-plane (Figure 2b). The wing like shape of the P3HT (100) peak (representing the angular orientation distribution of P3HT crystallites, known as mosaicity), is similar for all solvent mixtures (data not shown). For the determination of the associated spacing and coherence length of PCBM aggregates and P3HT crystallites, X-ray measurements were taken in specular reflection with a point detector (Figure 2c) and in grazing incidence. The diffraction profiles in out-of-plane direction along q_z and in-plane profiles along q_{xy} are depicted in Figure 2c and Figure 2d respectively. Figure 2c shows the P3HT (100) Bragg peak of the P3HT:PCBM blends dried in chloroform-indane, toluene-indane and o-xylene-indane 1:1 mixtures. From these profile plots the scattering plane spacing d and the crystalline correlation length L are determined from the Bragg peak position and the FWHM of the Bragg peak respectively. The profile plots were adapted with Gaussian fits for each Bragg reflection. Similar d_{100} spacing is

obtained for all solvent mixtures as well as a similar correlation length L_{100}, although slightly higher for the o-xylene-indane case (Table 1). This similarity of crystallinity can also be found in the in-plane data of Figure 2d, which reveals the same d_{020} spacing and the same correlation length L_{020} in π-π stacking direction except for the o-xylene-indane case where it is slightly lower (Table 1). The difference in the intensity of the (100) Bragg peak along q_z is due to the difference in thickness of the films. Hence, X-ray diffraction measurements reveal very similar crystallinity of the P3HT:PCBM films for the three solvent mixtures regardless of the differences in initial evaporation kinetics. This is a first indication that the approach of initially accelerated drying does not affect the final film morphology. In preceding work, such high (020) correlation length could only be reached at reduced drying temperature of 15°C (L_{020} = 11.8 nm for DCB). On the other hand the (100) correlation length is smaller for the investigated solvent mixtures as previously reported for DCB (L_{100} = 19.4 nm for DCB at 15°C drying temperature). [22]

We do not expect strong differences in the vertical gradients of P3HT:PCBM composition for the solvent mixtures driven by differences in their surface tensions. The higher volatile solvents exhibit comparable surface tensions of 27.5 mN/m, 28-28.5 mN/m and 29.5 mN/m for chloroform, toluene and o-xylene respectively. A nanoscale characterization of the film morphology was performed by AFM. Figure 3 shows 1×1 µm² phase images of the P3HT:PCBM films cast from the reference solvent DCB, pure indane and the solvent mixtures of chloroform, toluene and o-xylene with indane. The observed structures resemble those of P3HT lamellar fibrils. [25-27] While Figure 3a shows for DCB the finest fibril structure of all investigated films, the structure is coarser for indane processed films (Figure 3b). The similarity of the AFM phase images Figure 3b-e for films

processed from indane and its mixtures also suggests that the final indane dominated drying period governs morphology formation. Since the larger structure scale cannot be caused by longer assembly and crystallization times, they must originate from solvent specific properties. Such differences change the molecular conformation and the structural evolution due to specific solid-liquid interaction forces as for instance indicated by the increased PCBM solubility in indane compared to DCB.

3.3 Optoelectronic Properties for Different Solvent Mixtures

After having shown in AFM and GIXD measurements the structural similarity of P3HT:PCBM films processed from the above mentioned solvent mixtures, we now focus on the implications of the film structure on the optoelectronic properties of solar cells. The structural investigation revealed strong P3HT crystallinity in (100) direction perpendicular and in (020) π-π stacking direction along the substrate. Thus we expect strong vibronic shoulders in the absorption spectra due to the high amount of π-π-stacked P3HT molecules. This is confirmed by Figure 4 where the normalized absorption is plotted for pure DCB and indane as well as for all solvent mixtures. All absorption spectra feature strong vibronic shoulders (at about 605 nm) and a similar position of the main absorption peak (at about 500 nm) that indicates a similar conjugation length of the P3HT chains which is related to a similarly stretched conformation of P3HT.

The current density-voltage characteristics of P3HT:PCBM solar cells are depicted in Figure 5 for the fabrication from different solvent mixtures. The inset depicts the as cast devices and the main figure shows the same devices after thermal annealing. The poor device performance in Figure 5 prior to annealing is due to non optimized process

conditions probably caused by insufficient humidity desorption prior to the cathode depostition. After annealing the devices processed from the combination toluene-indane exhibit the highest power conversion efficiency although the bulk and surface morphology was similar to prior to the annealing step for all films cast from the different solvents (Figure 5a). Reasons for the dramatic difference in short circuit current density between chloroform (1.1 mA/cm²), o-xylene (5.8 mA/cm²) and toluene (8.2 mA/cm²) as higher volatile solvent components, cannot be found in the bulk microstructure or surface morphology since X-ray and AFM measurements have revealed similar properties for all films processed from the different solvents. We observed high P3HT crystallinity with similar amount of π-π stacking and similar crystalline orientation for all samples. In particular chloroform-indane leads to an extreme low short-circuit current and an S-shaped JV-curve although the bulk structure looks similar compared to the other films. Ruderer et al. observed the same effect for P3HT:PCBM solar cells processed from pure chloroform. They observed a strong vertical gradient with a serious enrichment of P3HT at the cathode interface which causes a strong barrier for electron extraction. [28] Although we can exclude a bilayer formation as it was suggested for pure chloroform according to our X-ray reflectivity measurements (data not shown), a similar trend of P3HT enrichment at the cathode interface might cause the similar JV-characteristic for chloroform mixed with indane.

Another set of solar cells was fabricated for the comparison of the most promising solvent mixture toluene-indane, the pure host solvent indane and the ideal reference solvent DCB (Figure 5b). Although DCB still provides the highest power conversion efficiency (Table 2), indane leads to comparable results. The practical disadvantage of pure indane with a

comparatively high surface tension of 34.9 mN/m is the poor wetting behavior, which can be improved by mixing with the discussed solvents that exhibit a lower surface tension. This improvement of film homogeneity due to solvent mixing can also be achieved for DCB with a surface tension of 37 mN/m.

In combination with toluene, the drying time can be reduced about 40% by generating a similar P3HT:PCBM crystallinity, absorption behavior and solar cell performance in comparison to DCB. A slight drawback is the increased series resistance which can be derived from the slope of the current density-voltage curve in the forward operation regime in Figure 5b. Overall, this indicates the solvent mixture toluene-indane as a suitable replacement of DCB for high throughput and large area fabrication of organic solar cells.

4. Conclusion

In order to accelerate the initial drying period without crossing the P3HT:PCBM solubility limit, we chose the solvent blending ratio of 1:1 of several higher volatile solvents blended with the host solvent indane which showed a transition to the slower host solvent evaporation kinetics at 95-96 wt% solvent fraction. The crystallinity and optic properties generated by this ratio was indeed comparable for chloroform, toluene and o-xylene combined with indane regardless of their vapor pressure. The combination of toluene-indane showed similar performance in comparison to pure indane and DCB by 40% reduced drying time. This identifies this blend as suitable replacement for DCB and makes it appropriate for large scale and high throughput OPV fabrication. This work further provides a systematic understanding of the correlation between solvent mixtures and their associated drying behavior that can aid the choice of solvent strategies.

Acknowledgement

The presented work was funded by the German Research Foundation (DFG) within the Priority Program 1355. We thank Ralf Weigel for his support in the MPI-MF beamline at ANKA. We acknowledge the European Synchrotron Radiation Facility for provision of synchrotron radiation facilities and Alexei Vorobiev for his support at ESRF. We further thank Hendrik Hölscher and the Karlsruhe Nano Micro Facility (KNMF) for the access to the AFM. This work was carried out in the framework of Holst Centre's shared research programs. B.S.H. thanks the Karlsruhe House of Young Scientists (KHYS) for financial support.

References

[1] R.F. Service, Outlook Brightens for Plastic Solar Cells, Science 332 (2011) 293

[2] F.C. Krebs, S.A. Gevorgyan, J. Alstrup, A roll-to-roll process to flexible polymer solar cells: model studies, manufacture and operational stability studies, J. Mater. Chem. 19 (2009) 5442-5451

[3] R. Steim, P. Schilinsky, S.A. Choulis, C.J. Brabec, Flexible polymer photovoltaic modules with incorporated organic bypass diodes to address module shading effects, Sol. Energy Mater. Sol. Cells 93 (2009) 1963–1967

[4] S.C. Gong, S.K. Jang, S.O. Ryu, H. Jeon, H.H. Park, H.J. Chang, Post annealing effect of flexible polymer solar cells to improve their electrical properties, Curr. Appl. Phys. 10 (2010) e192-e196

[5] Y. Galagan, J.E.J.M.Rubingh, R. Andriessen, C.C. Fan, P.W.M. Blom, S.C. Veenstra, J.M. Kroon, ITO-free flexible organic solar cells with printed current collecting grids, Sol. Energy Mater. Sol. Cells 95 (2011) 1339-1343

[6] D.J. Lipomi, B.C.K. Tee, M. Vosgueritchian, Z. Bao, Stretchable Organic Solar Cells, Adv. Mater. 23 (2011) 1771-1775

[7] B. O'Connor, K.P. Pipe, M. Shtein, Fiber based organic photovoltaic devices, Appl. Phys. Lett. 92 (2008) 193306

[8] Frederik C. Krebs, Polymer solar cell modules prepared using roll-to-roll methods: Knife-over-edge coating, slot-die coating and screen printing, Sol. Energy Mater. Sol. Cells 93 (2009) 465-475

[9] Frederik C. Krebs, Fabrication and processing of polymer solar cells: A review of printing and coating techniques, Sol. Energy Mater. Sol. Cells 93 (2009) 394-412

[10] F.C. Krebs, T. Tromholt, M. Jørgensen, Upscaling of polymer solar cell fabrication using full roll-to-roll processing, Nanoscale 2 (2010) 873-886

[11] B. Zimmermann, H.-F. Schleiermacher, M. Niggemann, U. Würfel, ITO-free flexible inverted organic solar cell modules with high fill factor prepared by slot die coating, Sol. Energy Mater. Sol. Cells 95 (2011) 1587-1589

[12] F.C. Krebs, J. Alstrup, H. Spanggaard, K. Larsen, E. Kold, Production of large-area polymer solar cells by industrial silk screen printing, lifetime considerations and lamination with polyethyleneterephthalate, Sol. Energy Mater. Sol. Cells 83 (2004) 293-300

[13] S.E. Shaheen, R. Radspinner, N. Peyghambrian, G.E. Jabbour, Fabrication of bulk heterojunction plastic solar cells by screen printing, Appl. Phys. Lett. 79 (2001) 2996-2998

[14] P. Kopola, T. Aernouts, S.Guillerez, H.Jin, M.Tuomikoski, A.Maaninen, J.Hast, High efficient plastic solar cells fabricated with a high-through put gravure printing method, Sol. Energy Mater. Sol. Cells 94 (2010) 1673–1680

[15] S.E. Shaheen, C.J. Brabec, N.S. Sariciftci, F. Padinger, T. Fromherz, J.C. Hummelen, 2.5% efficient organic plastic solar cells, Appl. Phys. Lett. 78 (2001) 841-843

[16] W. Yin, M. Dadmun, A New Model for the Morphology of P3HT/PCBM Organic Photovoltaics from Small-Angle Neutron Scattering: Rivers and Streams, ACS Nano 5 (2011) 4756–4768

[17] B.A. Collins, E. Gann, L. Guignard, X. He, C.R. McNeill, H. Ade, Molecular Miscibility of Polymer-Fullerene Blends, J. Phys. Chem. Lett. 1 (2010) 3160–3166

[18] J.A. Merlo, C.D. Frisbie, Field Effect Conductance of Conducting Polymer Nanofibers, J. Polym. Sci. Part. B: Polym. Phys. 41 (2003) 2674–2680

[19] V.D. Mihailetchi, H. Xie, B. Boer, L.M. Popescu, J.C. Hummelen, P.W.M. Blom, Origin of the enhanced performance in poly(3-hexylthiophene):[6,6]-phenyl C61-butyric acid methyl ester solar cells upon slow drying of the active layer, Appl. Phys. Lett. 89 (2006) 012107

[20] G. Li, V. Shrotriya, J. Huang, Y. Yao, T. Moriarty, K. Emery, Y. Yang, High-efficiency solution processable polymer photovoltaic cells by self-organization of polymer blends, Nat. Mater. 4 (2005) 864-868

[21] B. Schmidt-Hansberg, M. Sanyal, M.F.G. Klein, M. Pfaff, N. Schnabel, S. Jaiser, A. Vorobiev, E. Müller, A. Colsmann, P. Scharfer, D. Gerthsen, U. Lemmer, E. Barrena, W. Schabel, Moving through the phase diagram: morphology formation in solution cast polymer–fullerene blend films for organic solar cells, ACS Nano (submitted)

[22] M. Sanyal, B. Schmidt-Hansberg, M.F.G. Klein, A. Colsmann, C. Munuera, A. Vorobiev, U. Lemmer, W. Schabel, H. Dosch, E. Barrena, In Situ X-Ray Study of Drying-Temperature Influence on the Structural Evolution of Bulk-Heterojunction Polymer–Fullerene Solar Cells Processed by Doctor-Blading, Adv. Energy Mater. 1 (2011) 363–367

[23] B. Schmidt-Hansberg, M. Baunach, J. Krenn, S. Walheim, U. Lemmer, P. Scharfer, W. Schabel, Spatially resolved drying kinetics of multi-component solution cast films for organic electronics, Chem. Eng. Process. 50 (2011) 509-515

[24] B. Schmidt-Hansberg, M.F.G. Klein, K. Peters, F. Buss, J. Pfeifer, S. Walheim, A. Colsmann, U. Lemmer, P. Scharfer, W. Schabel, In situ monitoring the drying kinetics of knife coated polymer-fullerene films for organic solar cells, J. Appl. Phys. 106 (2009) 124501

[25] R. Zhang, B. Li, M.C. Iovu, M. Jeffries-El, G. Sauvé , J. Cooper, S. Jia, S. Tristram-Nagle, D.M. Smilgies, D.N. Lambeth, R.D. McCullough, T. Kowalewski, Nanostructure Dependence of Field-Effect Mobility in Regioregular Poly(3-hexylthiophene) Thin Film Field Effect Transistors, J. Am. Chem. Soc. 128 (2006) 3480-3481

[26] W.D. Oosterbaan, J.C. Bolsee, A. Gadisa, V. Vrindts, S. Bertho, J. DHaen, T.J. Cleij, L. Lutsen, C.R. McNeill, L. Thomsen, J.V. Manca, D. Vanderzande, Alkyl-Chain-Length-Independent Hole Mobility via Morphological Control with Poly(3-alkylthiophene) Nanofibers, Adv. Funct. Mater. 20 (2010) 792-802

[27] E.J.W. Crossland, K. Rahimi, G. Reiter, U. Steiner, S. Ludwigs, Systematic Control of Nucleation Density in Poly (3-Hexylthiophene) Thin Films, Adv. Funct. Mater. 21 (2011) 518-524

[28] M. Ruderer, S. Guo, R. Meier, H.Y. Chiang, V. Körstgens, J. Wiedersich, J. Perlich, S.V. Roth, P. Müller-Buschbaum, Solvent-Induced Morphology in Polymer-Based Systems for Organic Photovoltaics, Adv. Funct. Mater., DOI:10.1002/adfm.201100945

List of Tables:

Table 1: Structural data for P3HT and PCBM obtained from the GIXD data for films cast from different solvent mixtures at room temperature: spacings *d* associated with the (100) and (020) Bragg reflections of P3HT and those of PCBM and mean coherence length *L* along those crystallographic directions. Film thicknesses were in the range of 170-180nm.

Solvent	d_{100} [nm]	L_{100} [nm]	d_{020} [nm]	L_{020} [nm]	d_{PCBM} [nm]	L_{PCBM} [nm]
Chloroform-Indane	1.6	15.2	0.38	11.8	0.45	2.9
Toluene-Indane	1.6	15.2	0.38	11.8	0.45	2.9
o-Xylene-Indane	1.6	16.4	0.38	10.2	0.45	2.9

Table 2: Current density-voltage characteristics of P3HT:PCBM solar cells fabricated by doctor blading under ambient conditions from different solvents. With *d* as thickness, J_{sc} as short-circuit current density, V_{oc} as open circuit voltage, *FF* as fill factor and *PCE* as power conversion efficiency under mentioned illumination conditions with a spectral mismatch factor of 0.75. PB indicates an additional post bake for 5min at 130°C.

Solvent	*d* [nm]	J_{sc} [mA/cm²]	V_{oc} [V]	*FF* [-]	*PCE* [%]	PCE_{max} [%]
Toluene-Indane	225±60	5.5±3.0	0.41±0.03	0.32±0.25	1.0±0.6	2.0
Toluene-Indane + PB	225±60	7.4±1.0	0.53±0.06	0.41±0.05	1.5±0.4	2.1
DCB	265±150	3.8±1.8	0.48±0.03	0.53±0.03	1.0±0.6	1.9
DCB + PB	265±150	7.9±1.1	0.57±0.02	0.41±0.08	1.9±0.6	2.7

Figures

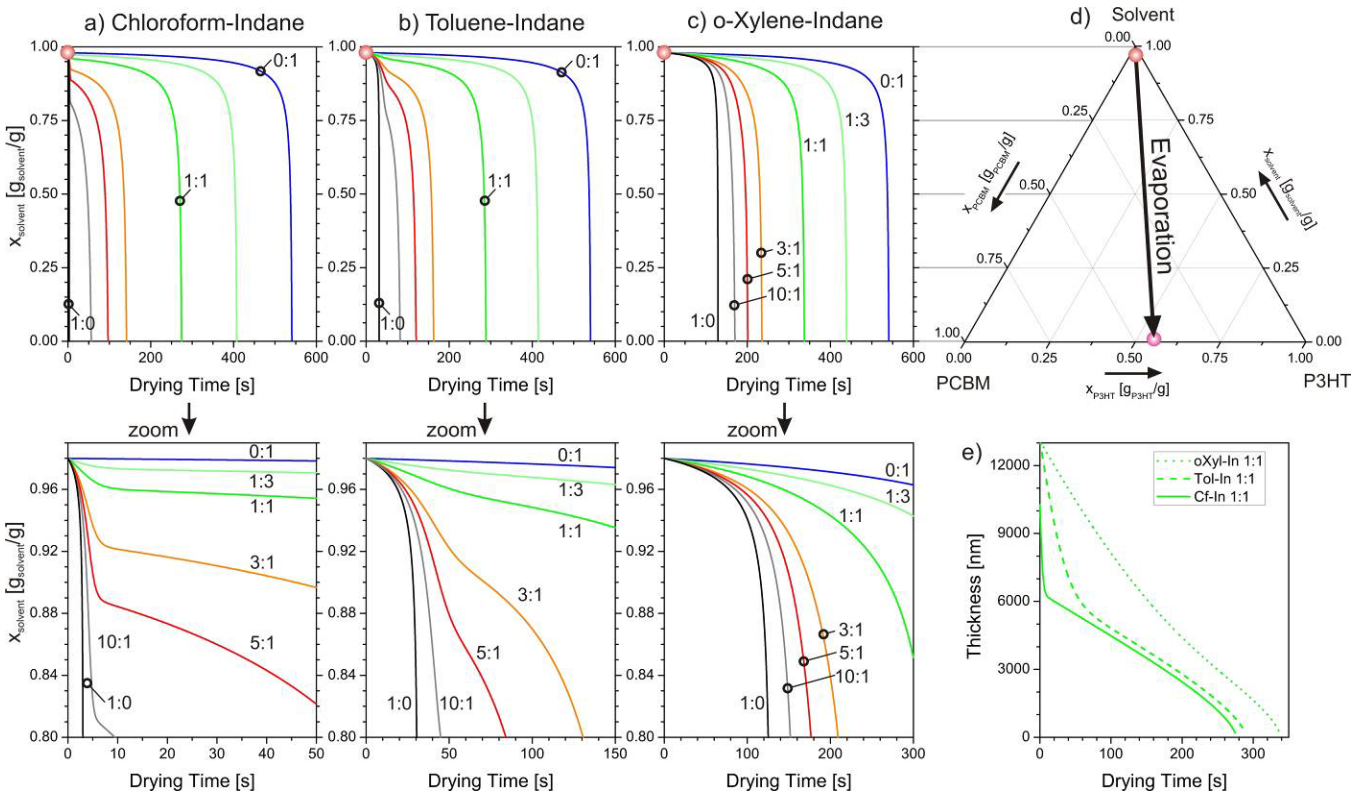

Figure 1: Calculated drying kinetics (constant rate period) of the solvent mixtures a) chloroform-indane, b) toluene-indane and c) o-xylene-indane for different solvent blending ratios (by weight) which are indicated in c). The top row shows the entire evolution while the bottom row depicts a zoomed view of the composition evolution. d) Corresponding drying path through ternary phase diagram of P3HT:PCBM (1:0.8) solution. e) Corresponding thickness evolution of each 1:1 solvent blending ratio. Drying conditions were chosen to 20°C drying temperature, 0.3m/s gas flow rate in horizontal plate geometry for 200nm dry film thickness and 2wt% initial solid fraction. In this figure both solvents are combined to an overall solvent fraction. The evaporation kinetics of pure DCB are comparable to those of pure indane due to the similar vapor pressure.

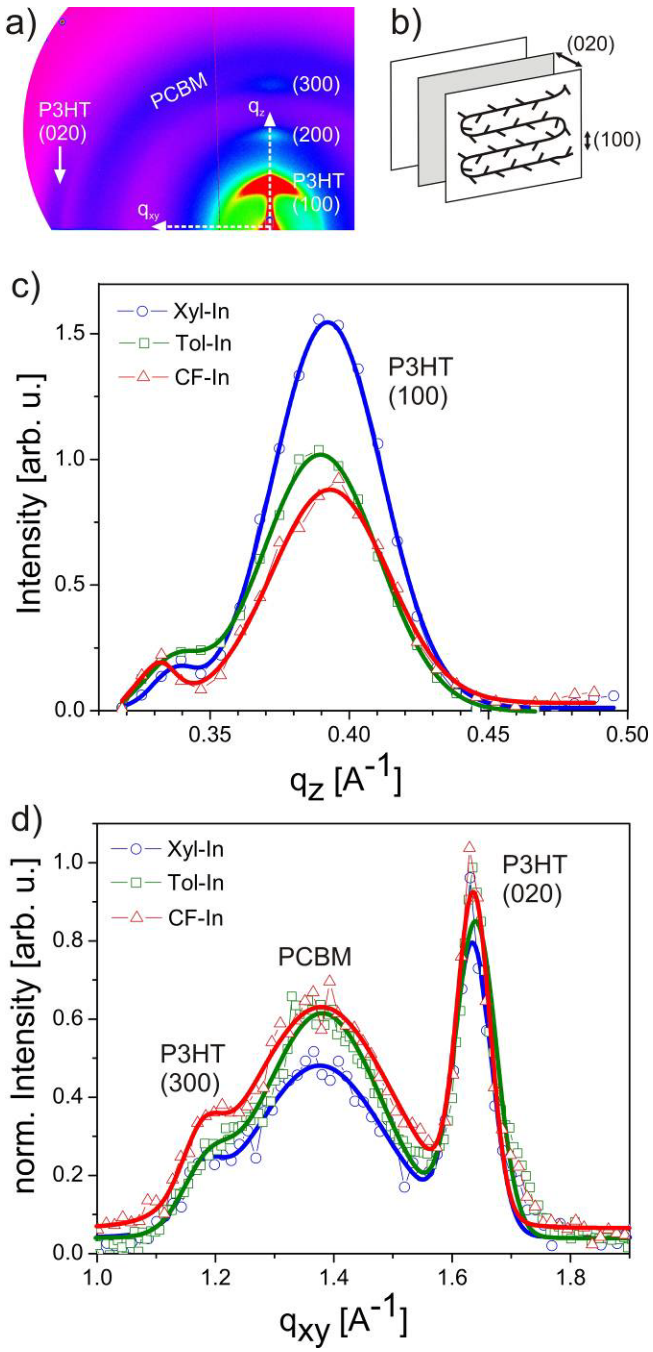

Figure 2: a) 2D GIXD diffraction pattern of P3HT:PCBM film cast from a toluene-indane mixture. b) Schematic unit cell of P3HT crystallites. c) Out-of-plane and d) in-plane X-ray diffraction profiles of P3HT:PCBM films cast from different solvent mixtures obtained by point detector measurements. Symbols represent experimental data and lines the appropriate Gaussian fits. The solvent blending ratios were for all combinations 1:1.

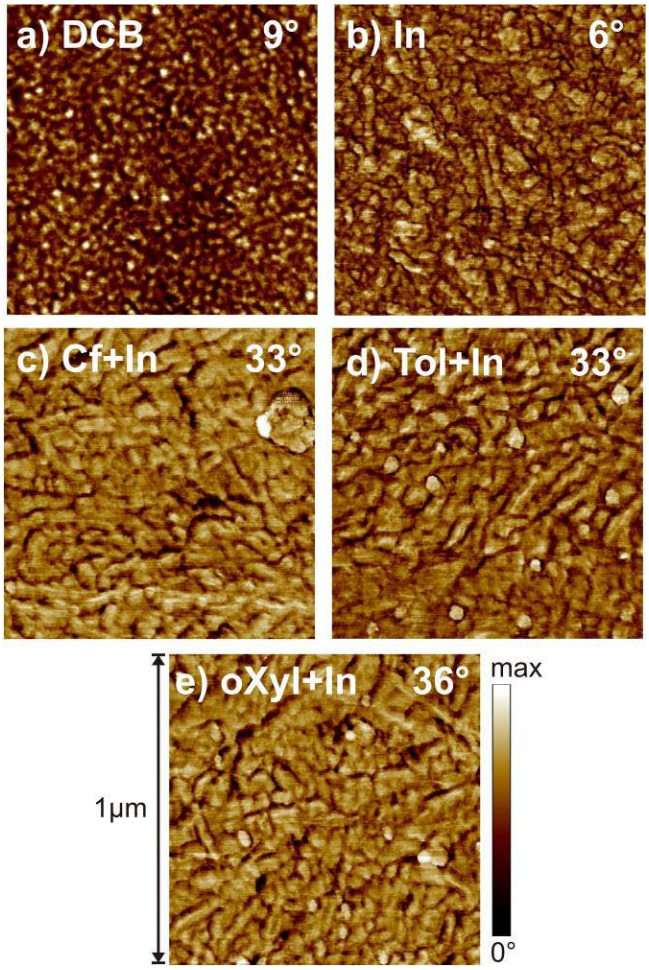

Figure 3: AFM phase images of P3HT:PCBM films cast by doctor blade from different solvents such as a) o-dichlorobenzene, b) indane, c) chloroform-indane, d) toluene-indane and e) o-xylene-indane at room temperature. The solvent blending ratio was for all cases 1:1 by volume. For clarification the image scale was adapted for each image differently as indicated in each image.

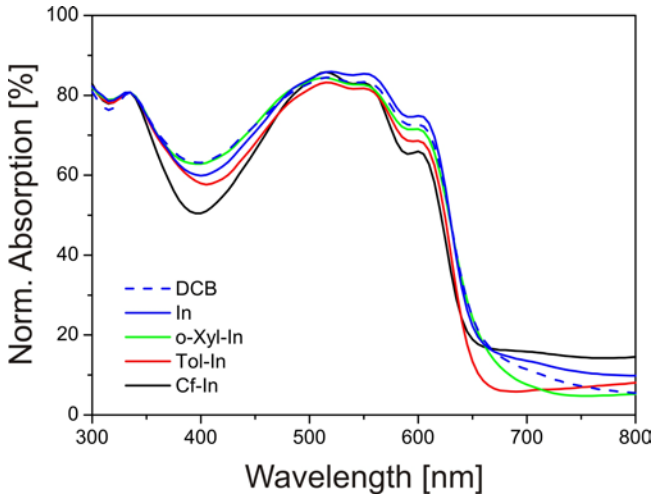

Figure 4: Absorption spectra of P3HT:PCBM (1:0.8) films cast from o-dichlorobenzene (DCB), indane (In), o-xylene-indane (o-Xyl-In), toluene-indane (Tol-In) and chloroform-indane (Cf-In). The solvent blending ratios were 1:1 for all combinations. Spectra are normalized to the PCBM absorption peak at 333nm.

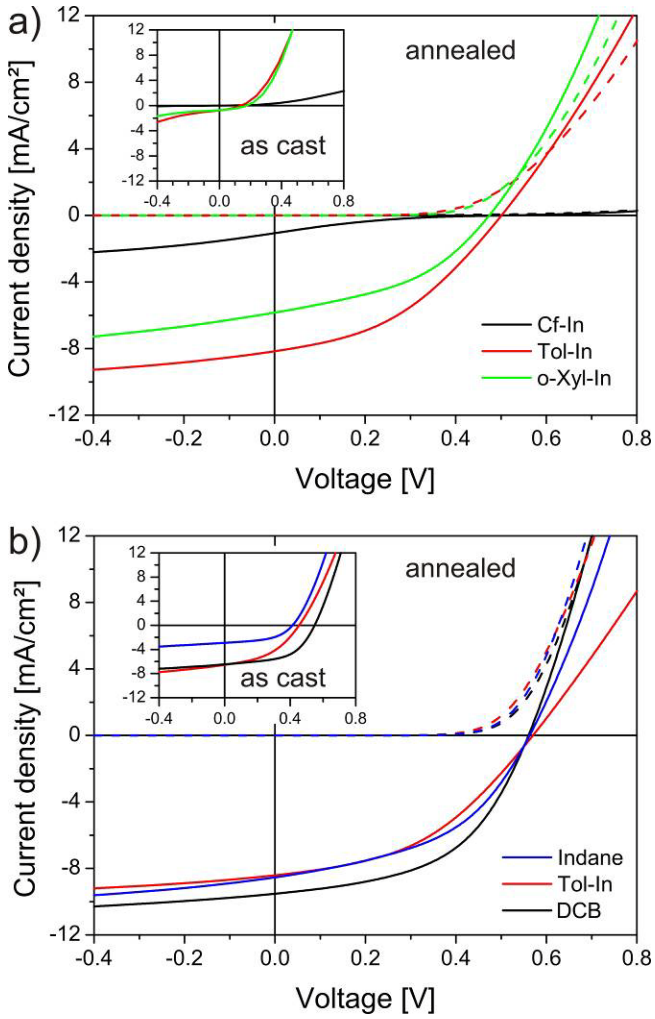

Figure 5: a) Typical current density-voltage characteristics of P3HT:PCBM (1:0.8) solar cells fabricated under ambient conditions by doctor blading and slow drying conditions from the solvent mixtures chloroform-indane (Cf-In), toluene-indane (Tol-In) and o-xylene-indane (o-Xyl-In) in 1:1 ratio for all solvents. The inset shows as cast devices and the main figure shows thermally annealed devices (5min, 130°C) respectively. b) Best current density-voltage characteristics of equally fabricated solar cells from pure indane (In), o-dichlorobenzene (DCB) and toluene-indane (Tol-In). Solid lines represent conditions under illumination while dashed lines are measured under dark conditions.